

The influence of metal ions on the adsorption of octyl hydroxamic acid in the flotation of bastnaesite and the adsorption mechanism

Rongxiang Liu ¹, Jie Li ², Zhao Cao ¹, Wenqiang Shi ³

¹ Mining and Coal School of Inner Mongolia University of Science and Technology, Baotou, 014010, China

² Rare-Earth School of Inner Mongolia University of Science and Technology, Baotou, 014010, China

³ Inner Mongolia Baotou Steel Union Co., Ltd. Barun Mining Branch, Baotou, 014010, China

Corresponding author: yjslijie@sohu.com (Li Jie)

Abstract: The influence mechanism of metal ions on the adsorption of octyl hydroxamic acid (OHA) by bastnaesite in a flotation system was studied by flotation experiments, adsorption capacity tests, X-ray photoelectron spectroscopy (XPS) characterization, and density functional theory (DFT) study. From the experimental results, it can be seen that the flotation and the adsorption capacity tests showed that the single metal ions Ca^{2+} , Ba^{2+} , and Fe^{3+} promoted the flotation recovery of bastnaesite, and the order of their ability was $\text{Ba}^{2+} > \text{Fe}^{3+} > \text{Ca}^{2+}$. The addition of mixed metal ions inhibited the adsorption of OHA on the surface of bastnaesite, resulting in a decrease in the flotation recovery of bastnaesite. The XPS analysis showed that the N concentration on the surface of bastnaesite after single metal ion action was significantly higher than that without metal ion action, while the N concentration on the surface of bastnaesite after mixed metal ion action was significantly lower than that without metal ion action. When Ca^{2+} , Ba^{2+} , and Fe^{3+} ions were added, new peaks appeared at 401.24 eV, 397.68 eV, and 397.19 eV in the N1s fitting peaks, respectively, which may be caused by the formation of N-M (OH) chemical bonds between $\text{M}(\text{OH})^+$ (M: Ca^{2+} , Ba^{2+} , Fe^{3+}) and nitrogen atoms in OHA. This indicated that metal ions Ca^{2+} , Ba^{2+} , and Fe^{3+} form metal chelated with nitrogen atoms in OHA. The DFT study on the (100) surface of bastnaesite also showed that the doping of metal ions showed a stronger spontaneity and enhanced adsorption capacity due to the decrease of adsorption energy between OHA and bastnaesite surface. There were two adsorption sites of bastnaesite, one is that the Ce atom adsorbs two oxygen atoms of OHA to form a five-membered chelate, and the other adsorption site was that O-M(OH) on bastnaesite interacts with OHA; Therefore, the configuration of the oxygen atom adsorption site is O-M-O-N bond, during which $\text{M}(\text{OH})^{n+(n-1,2)}$ loses OH⁻, and the N-O-H chemical bond on OHA loses H⁺ to form an H₂O molecule, a typical dehydration reaction, so the adsorption is more stable. Therefore, the surface of bastnaesite has two adsorption forms with OHA, one is R-NH-O-M-CeFCO₃ and R-NH-O-CeFCO₃.

Keywords: bastnaesite, flotation, metal ions, octyl hydroxamic acid, adsorption mechanism

1. Introduction

Rare earth elements have unique fluorescence, magnetic, and chemical properties due to their special electronic structure, which are widely used in the military, agriculture, metallurgy, petrochemical, and other fields (Dushyantha et al., 2020). With the development of science and technology, rare earth plays an increasingly important role in promoting traditional industries and developing high-tech industries. Fluorocarbon cerium ore is the main source of rare earth; Bayan Obo mine in China and the Mountain Pass mine in the United States are the main deposits of bastnaesite (Long et al., 2012; Jordens et al., 2013).

As a common method for efficient enrichment of bastnaesite, flotation is widely used in the beneficiation practice of bastnaesite (Xu et al., 2020). Studies have shown that the two main collectors used in the flotation of bastnaesite are fatty acids and hydroxamic acids. Among them, the specific selectivity of hydroxamic acid to rare earth cations is better than that of fatty acids, so hydroxamic acid is widely used in bastnaesite flotation (Xu et al., 2023). On this basis, scholars have further explored new

collectors and inhibitors to improve the separation effect of bastnaesite and associated minerals (Cao et al., 2019; Qi et al., 2020; Wang et al., 2020; Yu et al., 2020). In addition, Liu et al. (2023) published a review recently, which summarized the previous research results of rare earth mineral flotation, including a detailed description of various reagents (collectors, surface activators, inhibitors, and foaming agents) used in bastnaesite flotation. Of course, in complex flotation systems, some mineralogical factors (such as lattice impurities, mineral dissolution, and release of fluid inclusions, etc.) and pulp environment (such as flotation reagents, water quality, grinding media, etc.) are important sources of metal ions, which usually affect the flotation behavior of minerals (Yin et al., 2021). According to the different properties of metal ions and collectors, metal ions can promote or block the adsorption of collectors on mineral surfaces, thereby affecting the recovery of target minerals (Chen et al., 2017; Wei et al., 2019; Cao et al., 2021). Therefore, the role of metal ions in the flotation of bastnaesite has also been studied (Cao et al., 2018; Cao et al., 2019; Lin et al., 2020).

Among many metal ions, metal ions have been studied by many researchers as the inevitable ions in grinding. Studies have shown that there are a variety of metal ions in REE ore pulp (Moonchul et al., 2022; Yu et al., 2023), and metal ions have a great influence on mineral flotation (Espiritu ERL et al., 2018). Based on this, the selection of collectors is more important. The selectivity of fatty acid and phosphoric acid collectors is lower than that of hydroxamic acid. The hydroxyl complex ions produced by the hydration of metal ions by hydroxamic acid functional groups produce chemical adsorption in the form of multiple chelating rings (Xu et al., 2023), which is more conducive to the flotation of rare earth minerals in a variety of metal ion pulps. For example, by adding Fe^{3+} in advance, Fe^{3+} can combine with the hydroxyl group on Sn-OH to form adsorption sites, promote the reaction between BHA and iron atoms to form Fe-BHA complexes and activate cassiterite flotation (Tian et al., 2018). Zheng et al. (2021) considered that the $-\text{O}_{\text{surf}}-\text{Fe}$ group of bastnaesite formed by the reaction of Fe^{3+} with the surface O atom on the surface of bastnaesite is a new active site for collector adsorption. Yu et al. (2022) found that $\text{Pb}(\text{OH})^+$ formed by lead ions and iron hydroxyl compounds increased the adsorption sites of OHA on ilmenite by dehydration reaction, thereby improving the floatability of minerals. Ca^{2+} can activate minerals such as quartz (Chen et al., 2012), kyanite (Zhang et al., 2014), dolomite (Huang et al., 2021), and sphalerite (Dávila-Pulido et al., 2015). Calcium ions are mostly activated in the anion system when the pH is 8~12. The mechanism of metal ion activation is still controversial, which is mainly based on the precipitation and adsorption of hydroxyl complexes or hydroxides to increase the active sites of minerals (Cao et al., 2018).

At present, there are some studies on the interaction between metal ions and bastnaesite surface (Cao et al., 2018; Cao et al., 2019). However, these studies mainly consider metal ions and the surface of bastnaesite, while there are few studies on collectors, and there are few studies on the adsorption of mixed metal ions on bastnaesite collectors. Therefore, in the process of bastnaesite flotation, the influence of metal ions on collectors, especially the interaction mechanism between metal ions, collectors, and bastnaesite surface, remains to be further studied. Only an in-depth study of the mechanism can provide more valuable theoretical guidance for the actual flotation of bastnaesite.

In the flotation of bastnaesite, metal ions, especially Ca^{2+} , Ba^{2+} , and Fe^{3+} , are inevitable in the pulp (Chen et al., 2017; Wei et al., 2019; Yin et al., 2021; Gao et al., 2021). On this basis, the effects of Ca^{2+} , Ba^{2+} , and Fe^{3+} on the surface adsorption of bastnaesite by one or more metal ions were studied by micro-flotation test, adsorption experiment, X-ray photoelectron spectroscopy (XPS) measurement, and density functional theory (DFT) calculation using octyl hydroxamic acid collector.

2. Materials and methods

2.1. Materials

The pure mineral sample of bastnaesite was taken from Bayan Obo mine. Iron and other impurities in the sample were removed by gravity separation. After magnetic separation and wet screening by an artificial magnetic rod, the ore powder with a particle size of $-75+38 \mu\text{m}$ was collected for the flotation tests. Some samples were further ground to about $-5 \mu\text{m}$ for adsorption mechanism analysis. The purity of bastnaesite was analyzed by chemical composition analysis as presented in Table 1 and by X-ray diffraction pattern as shown in Fig. 1. The results show that the purity of these minerals is greater than 95%, which meets the pure mineral test and detection analysis.

The pH adjustment was performed using analytically pure HCl and NaOH from Sinopharm Group (China). Analysis of metal ions selected pure FeCl₃, CaCl₂, BaCl₂, purity 99.9%, from Lianyungang (China). Octyl hydroxamic acid (OHA) was used as a collector in the flotation test, with a purity of 99.9 %, from Shanghai Yuanye Biotechnology Co., Ltd. (China). Methyl isobutyl methanol (MIBC) was used as a frother, with a purity of 99%, from Shanghai Yuanye Biotechnology Co., Ltd. (China). Type I deionized water (DI) prepared by Mil-9 water system was used in all experiments. The resistivity of the water was 18.2 MΩ · m. The manufacturer was Sigma Odrich (Shanghai) Trading Co., Ltd.

Table 1. Chemical composition of bastnaesite mineral samples (wt. %)

Sample	REO	CaO	TFe	SiO ₂	BaO	ThO ₂
<i>Bastnaesite</i>	73.65	0.64	1.22	0.13	0.39	0.063

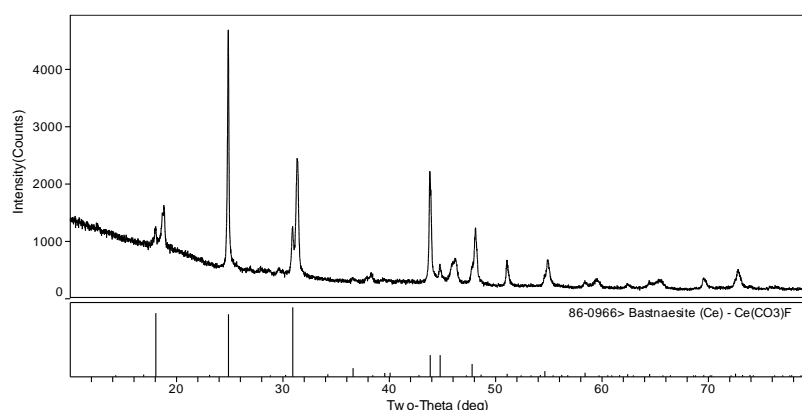


Fig. 1. XRD patterns of pure bastnaesite minerals

2.2. Methods

2.2.1. Flotation tests

Micro-flotation test was carried out in XFGII flotation equipment (Jilin Exploration Machinery Factory, China). In the single mineral flotation test, 2 g pure minerals and 37 cm³ DI water were poured into the flotation tank and stirred at a speed of 1940 rpm. After stirring for 2 min, the pH regulator (HCl or NaOH) was added to adjust the required pH value within 2 min. Then, the metal ions were added in turn, and the collector OHA was added to make each reagent interact with the mineral for 3 min. Then, the froth was scraped out for 3 min. The concentrate and tailings products were collected, dried, and weighed, respectively. Each experiment was repeated three times and the average was reported.

2.2.2. Adsorption tests

The residual concentration method was used to determine the adsorption amount of inorganic modifier on the mineral surface: 2 g of ore sample with particle size less than 0.074 mm was weighed and added to the flotation machine of the inflatable hanging tank, 40 cm³ DI water was added, and the modifier was added. Stir for 30 min; the adjusted pulp was centrifuged in a centrifuge, and the upper layer was taken overnight. The ICP spectrometer was used for elemental analysis to obtain the content of the corresponding collector OHA in the supernatant. The content adsorbed on the surface of pure minerals can be obtained by subtraction.

2.2.3. XPS measurement and analysis

The XPS spectra of bastnaesite samples before and after the adsorption of reagents were measured to determine the changes in the chemical environment of elements on the mineral surface. For each test, the test sample (particle size from 75×38 μm) is treated the same as the single mineral flotation. The treated samples were filtered, washed with pure water, and dried. The XPS test used the Escalab250 xi instrument (Thermo Fisher Science, USA). The C-1s peak at 284.8 eV (C-C) was used as the standard

binding energy for calibration. Avantage6.0 software was used to optimize the test data, curve fitting, and analysis.

2.2.4. DFT calculation

DFT is widely used as an effective quantum method to study the interaction between reagents and minerals at the atomic level (Cudi et al., 2018; Liu et al., 2020). In addition, DFT theory was also used in the study of bastnaesite and hydroxamic acid flotation. For example, Sarvaramini et al. (2016) studied the interaction between hydroxamic acid and solvated cerium oxide in the flotation process of bastnaesite by DFT calculation. Wanhala et al. studied the adsorption mechanism of hydroxamic acid on the surface (Wanhala et al., 2019). These studies prove the feasibility of using DFT to study the flotation of bastnaesite in a hydroxamic acid system. Therefore, based on DFT, CASTEP studies carried out first-principles periodic calculations to study the effects of Ca^{2+} , Ba^{2+} , and Fe^{3+} on the flotation of bastnaesite and its mechanism. Firstly, CASTEP periodic DFT was used in Materials Studio to cut the original surface of bastnaesite with a plate-like surface layer from the optimized bastnaesite body, and the ideal surface structure of bastnaesite was obtained. The surface structure of bastnaesite doped with impurity metal ions was optimized again. By calculating the adsorption and electronic structure of Ca^{2+} , Ba^{2+} , and Fe^{3+} on the surface of bastnaesite and OHA, the effects of Ca^{2+} , Ba^{2+} , and Fe^{3+} on the adsorption agent on the surface of bastnaesite were analyzed.

Throughout the study, the ultrasoft pseudopotential is used to characterize the interaction between valence electrons and ionic nuclei. All calculated convergence criteria (a) have an energy tolerance of 1.0×10^{-5} eV/atom, (b) a maximum tolerance of 0.03 eV/Å, (c) a maximum stress tolerance of 0.05 GPa, (d) a maximum displacement tolerance of 0.001 Å, and (e) an SCF tolerance of 1×10^{-6} eV/atom.

3. Results and discussion

3.1. Results

3.1.1. Effect of metal ions on bastnaesite flotation

When the concentration of octyl hydroxamic acid was 5×10^{-4} mol/dm³, the pulp pH was 9, the amount of MIBC frother was 30 ppm, and the effect of metal ions in different concentrations on the flotation of bastnaesite was added. The results are shown in Fig. 2.

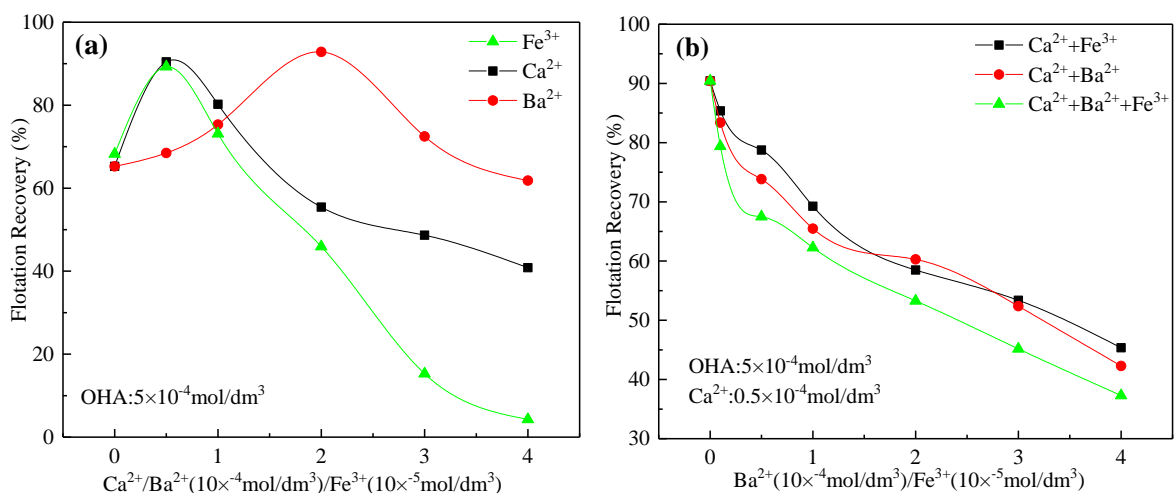


Fig. 2. Effect of metal ion concentration on flotation recovery of bastnaesite: (a) single metal ions, (b) mixed metal ions

The effect of single metal ions on the recovery rate of bastnaesite is shown in Fig. 2(a). It shows that the recovery rate of bastnaesite increases first and then decreases with the increase of metal ion concentration. When the concentrations of Ca^{2+} , Ba^{2+} , and Fe^{3+} are 0.5×10^{-4} mol/dm³, 2×10^{-4} mol/dm³, and 0.5×10^{-5} mol/dm³, respectively, the recovery rates are 88.27%, 92.83%, and 90.43% respectively, indicating that the ability to promote the recovery rate of bastnaesite is $\text{Ba}^{2+} > \text{Fe}^{3+} > \text{Ca}^{2+}$. Fig. 2(b) shows

the effect of mixed metal ions on the recovery rate of bastnaesite. It can be seen that with the increase in the concentration of mixed metal ions, the recovery rate gradually decreases. The most influential is the presence of $\text{Ca}^{2+}/\text{Ba}^{2+}/\text{Fe}^{3+}$ at the same time. It shows that the addition of mixed metal ions will inhibit the flotation recovery of bastnaesite. It may be that the increase in metal ion concentration will cause competitive adsorption and inhibit OHA adsorption on the surface of bastnaesite. The decrease of surface hydrophobicity of bastnaesite leads to a decrease in recovery rate.

3.1.2. Effect of metal ions on the adsorption of OHA on the surface of bastnaesite

Fig. 3 shows the effect of metal ion concentration on the adsorption of OHA on the surface of bastnaesite. It can be seen from the Fig. that both the concentration of single metal ions and the concentration of mixed metal ions have a great influence on the adsorption of OHA on the surface of bastnaesite. From Fig. 3 (a), it can be seen that the single metal ions Ca^{2+} , Ba^{2+} , and Fe^{3+} at a certain concentration will promote the adsorption amount of OHA on the surface of bastnaesite. When Ca^{2+} is $0.5 \times 10^{-4} \text{ mol/dm}^3$, the adsorption amount of OHA is the largest, which is 9.99 mg/g; when Ba^{2+} is $2 \times 10^{-4} \text{ mol/dm}^3$, the adsorption capacity of OHA is the largest, which is 11.58 mg/g. The maximum adsorption capacity of OHA was 10.27 mg/g when Fe^{3+} was $0.5 \times 10^{-4} \text{ mol/dm}^3$. It can be seen from Fig. 3(b) that the adsorption capacity of OHA was inhibited by the three mixed metal ions at a certain concentration ratio, and the combination of $\text{Ca}^{2+}/\text{Ba}^{2+}/\text{Fe}^{3+}$ showed the greatest inhibitory effect on OHA. Comparing Figs. 3(a) and (b), it can be seen that single metal ions can promote the flotation recovery of bastnaesite, especially Ba^{2+} had the largest adsorption capacity for bastnaesite, while mixed metal ions showed an adverse effect on bastnaesite, inhibiting the adsorption of OHA on the surface of bastnaesite, which is consistent with the above flotation test results.

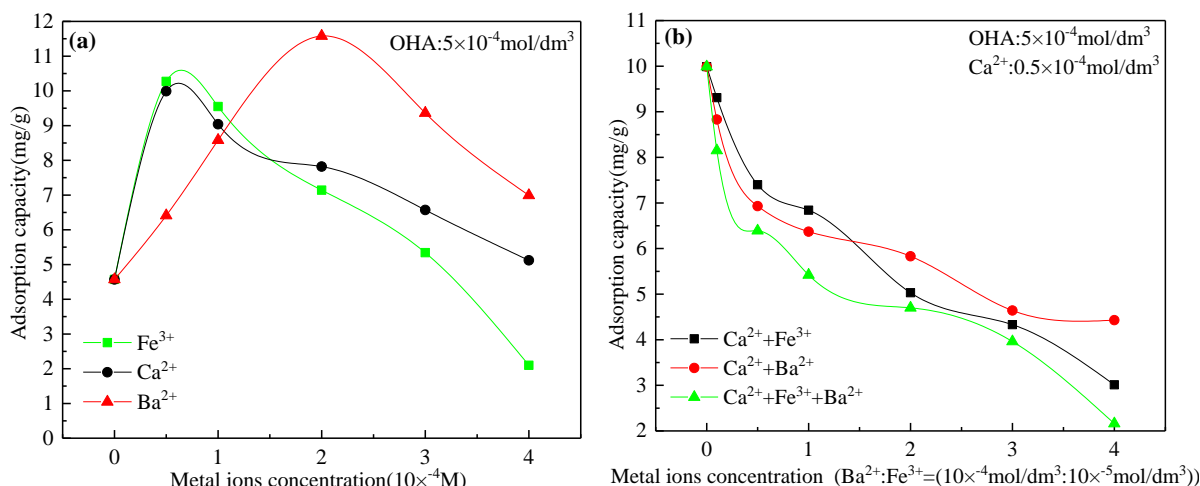


Fig. 3. Effect of metal ion concentration on adsorption of OHA on bastnaesite surface: (1) single metal ion, (2) mixed metal ions

3.1.3. XPS results

Fig. 4 is the XPS full spectrum of bastnaesite before and after the action of metal ions and OHA collector. In the test conditions, OHA collector ($5 \times 10^{-4} \text{ mol/dm}^3$), the single metal concentration of Ca^{2+} ($0.5 \times 10^{-4} \text{ mol/dm}^3$), Ba^{2+} ($2 \times 10^{-4} \text{ mol/dm}^3$), Fe^{3+} ($0.5 \times 10^{-5} \text{ mol/dm}^3$), mixed metal ion concentration of $\text{Ca}^{2+}/\text{Fe}^{3+}$ ($0.5 \times 10^{-4} \text{ mol/dm}^3/0.5 \times 10^{-5} \text{ mol/dm}^3$), $\text{Ca}^{2+}/\text{Ba}^{2+}$ ($0.5 \times 10^{-4} \text{ mol/dm}^3/2 \times 10^{-4} \text{ mol/dm}^3$), $\text{Ca}^{2+}/\text{Ba}^{2+}/\text{Fe}^{3+}$ ($0.5 \times 10^{-4} \text{ mol/dm}^3/0.5 \times 10^{-4} \text{ mol/dm}^3/0.5 \times 10^{-5} \text{ mol/dm}^3$).

Fig. 4(a) is the XPS full spectrum of single metal ions before and after the adsorption of OHA on bastnaesite, and Fig. 4(b) is the XPS full spectrum of mixed metal ions before and after the adsorption of OHA on bastnaesite. Table 2 presents the different atomic concentrations on the surface of bastnaesite before and after the adsorption of OHA on bastnaesite. It can be seen from Figs. 4(a) to (b) that N element appears on the surface of bastnaesite after the action of the agent, Ca, Ba, and Fe elements appear after the action of a single metal ion, and two or three metal ion elements appear simultaneously after the action of mixed metal ions. It can be seen from Table 2 that the N element after OHA is 2.86%, the N

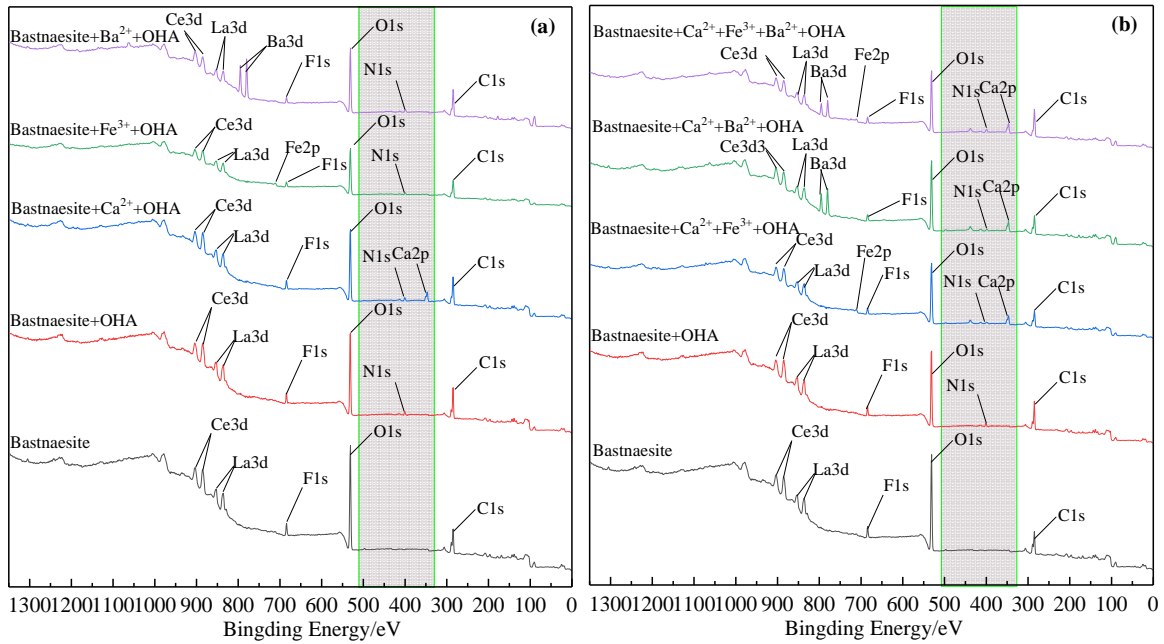


Fig. 4. XPS full spectrum of bastnaesite before and after the action of metal ions and OHA collectors (a) Single metal ions, (b) Mixed metal ions

Table 2. Different atomic concentrations of bastnaesite surface before and after the action of metal ions and OHA collectors

Samples	Surface Atomic Composition (%)								
	C	O	Ce	La	F	N	Ca	Fe	Ba
Bastnaesite	38.80	49.85	3.85	3.12	4.38	-	-	-	-
Bastnaesite + OHA	42.47	43.12	4.19	3.73	3.63	2.86	-	-	-
Bastnaesite + Ca ²⁺ + OHA	43.60	39.74	3.77	3.18	3.52	3.12	3.07	-	-
Bastnaesite + Ba ²⁺ + OHA	45.44	37.40	3.54	2.26	2.97	3.87	-	-	4.53
Bastnaesite + Fe ³⁺ + OHA	46.05	41.03	2.26	2.70	3.67	3.34	-	0.95	-
Bastnaesite + Ca ²⁺ + Fe ³⁺ + OHA	37.05	45.67	3.94	3.02	3.47	2.32	3.77	0.76	-
Bastnaesite + Ca ²⁺ + Ba ²⁺ + OHA	37.33	43.47	3.77	2.92	3.33	2.21	3.58	-	3.40
Bastnaesite + Ca ²⁺ + Ba ²⁺ + Fe ³⁺ + OHA	36.40	42.79	3.86	2.94	3.29	2.19	2.94	1.18	1.89

elements on the surface of bastnaesite after Ca²⁺, Ba²⁺, and Fe³⁺ are 3.12%, 3.87% and 3.34%, and the N elements on the surface of bastnaesite after Ca²⁺/Fe³⁺, Ca²⁺/Ba²⁺ and Ca²⁺/Ba²⁺/Fe³⁺ are 2.32%, 2.21% and 2.19%. It can be seen that the N concentration on the surface of bastnaesite after single metal ion action is significantly higher than that without metal ion action. The bastnaesite after the action of mixed metal ions is significantly lower than the bastnaesite without the action of metal ions. It shows that after the mixed metal ions act on the bastnaesite, too many metal ions compete for adsorption, which is not conducive to the flotation of bastnaesite, and a single metal ion is beneficial to the flotation of bastnaesite.

Fig. 5 (a) is the narrow spectrum of Ce3d element in bastnaesite before and after chemical action. There are two groups of Ce3d spectra, Ce3d_{3/2} and Ce3d_{5/2}, respectively. The higher binding energy is 905.29 eV, 902.93 eV, 899.80 eV, 896.49 eV, and the lower binding energy is 885.09 eV, 881.83 eV. After the bastnaesite was treated with OHA, the Ce-O bond binding energy of Ce3d orbital was shifted, and the shift value was 0.2~0.72 eV (greater than the instrument error), and a new fitting peak appeared at 886.95 eV, which may be the formation of Ce-N. It shows that the collector transfers electrons to the surface of bastnaesite, that is, the OHA collector undergoes chemical adsorption at the Ce atom. The Ce3d peaks of OHA adsorption on bastnaesite treated by single metal ions Ca²⁺, Ba²⁺, Fe³⁺ and mixed metal ions Ca²⁺/Fe³⁺, Ca²⁺/Ba²⁺, and Ca²⁺/Ba²⁺/Fe³⁺ show that the Ce3d orbital Ce-O bond binding energy has a large offset, and the offset value is 0.2~2.48 eV (greater than the instrument error), which is much larger than the offset of bastnaesite treated only by OHA, indicating that metal ions affect the

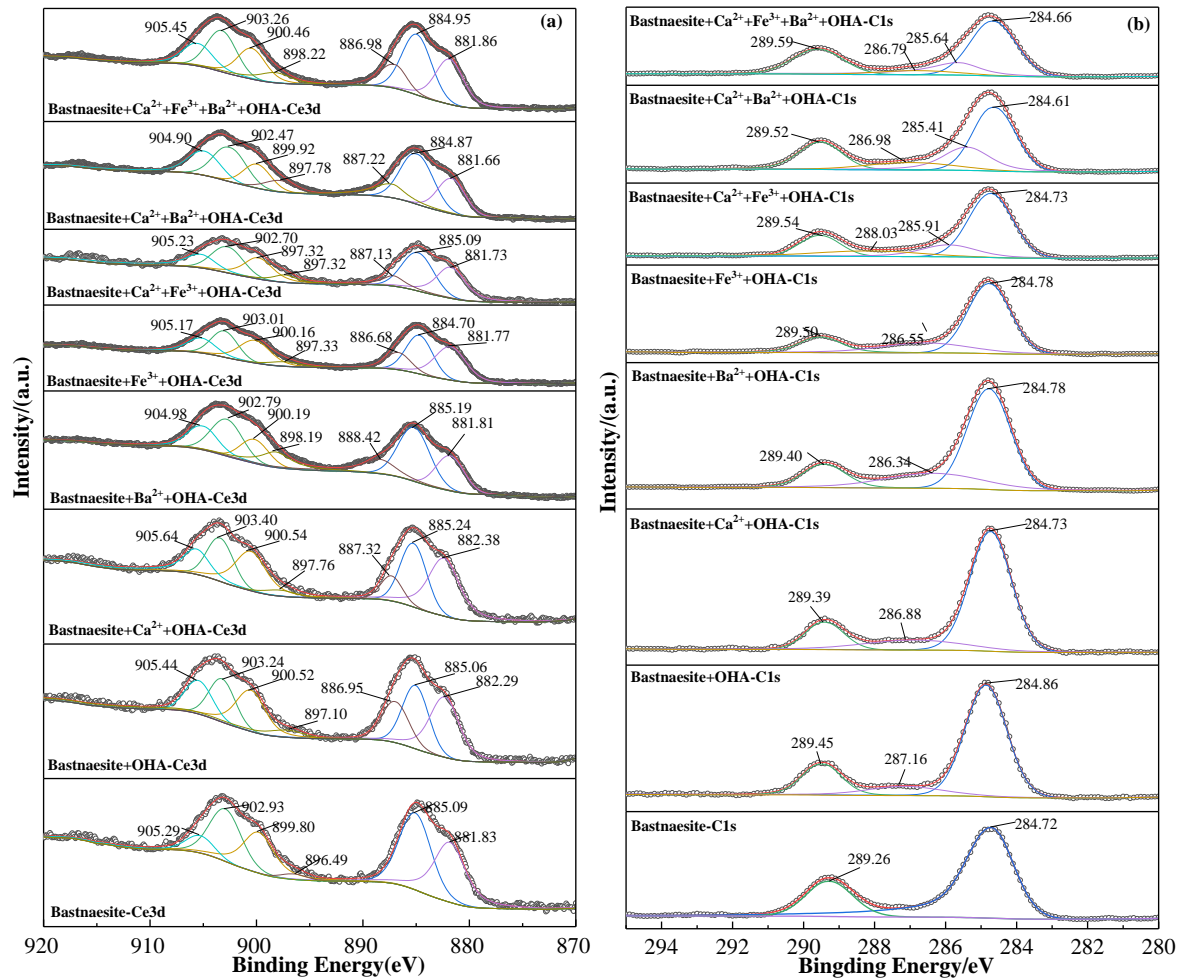


Fig. 5. The narrow-spectrum scanning fitting spectra of the elements on the surface of bastnaesite minerals before and after the action of reagents: (1) Ce3d; (2) C1s

adsorption of OHA by bastnaesite. From the ordinate, the photoelectron intensity of Ce3d changes, and the photoelectron intensity decreases after the action of metal ions. It may be that metal ions and OHA collectors are adsorbed on the surface of bastnaesite, which dilutes the concentration of Ce3d elements on the surface, resulting in a decrease in the photoelectron intensity of Ce3d, indicating that the adsorption capacity of metal elements increases.

Fig. 5(b) is the narrow spectrum of C1s elements before and after the action of the agent. The two characteristic peaks of pure bastnaesite, 284.72 eV and 289.26 eV, are attributed to CO_3^{2-} carbon pollution (Li et al., 2019). After the action of the collector, a new C-O peak is generated at the binding energy of 287.16 eV. After the single metal ions Ca^{2+} , Ba^{2+} , and Fe^{3+} acted on the bastnaesite, the new peak C-O shifted, and the offset was 0.28-0.72 eV. After the mixed metal ions $\text{Ca}^{2+}/\text{Fe}^{3+}$, $\text{Ca}^{2+}/\text{Ba}^{2+}$, and $\text{Ca}^{2+}/\text{Ba}^{2+}/\text{Fe}^{3+}$ act on the bastnaesite, two new peak-fitting peaks are formed. The results are shown in Fig. 5(2), which indicates that the metal ions affect the structure of OHA adsorbed by bastnaesite. It may be that the metal ions Ca^{2+} , Ba^{2+} , and Fe^{3+} adsorb on the surface of bastnaesite and adsorb with OHA, resulting in a change in bond energy.

Fig. 6(a) shows the fitting spectrum of the narrow spectrum of O1s on the surface of bastnaesite before and after the action of the agent. Only 531.03 eV of bastnaesite is the Ce-O fitting peak. The Ce-O fitting peak shifted by 0.12 eV after the action of the reagent OHA, and a new fitting peak was also generated at 531.88 eV, which was the O-N bond in the reagent OHA, indicating that the collector OHA was adsorbed on the surface of bastnaesite. When metal ions and OHA are introduced into bastnaesite, the surface O1s of bastnaesite consists of three peaks, which are from O-M (M is a metal atom), O-N, and Ce-O, respectively. O-M bond is the dominant component of metal ions adsorbed on the surface of bastnaesite, forming Ca-O, Ba-O, and Fe-O chemical bonds. The single metal ions Ca^{2+} , Ba^{2+} , Fe^{3+} , and

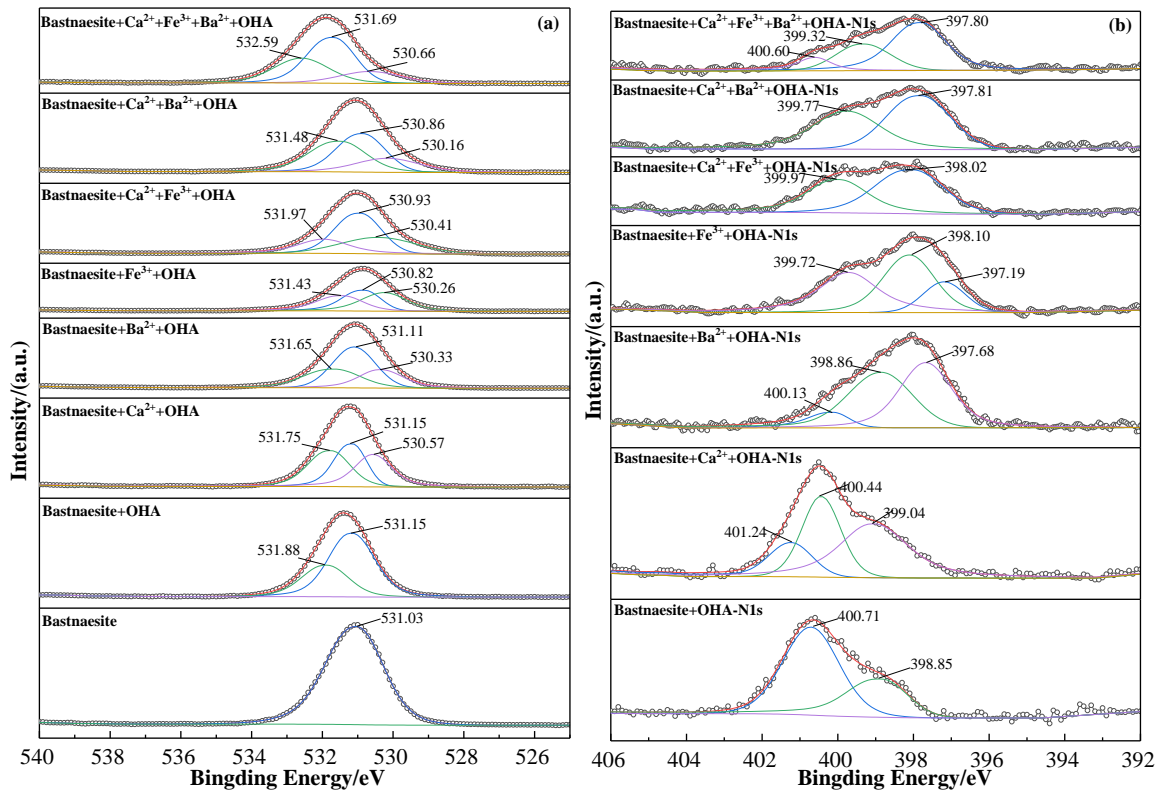


Fig. 6. The narrow-spectrum scanning fitting spectra of elements on the surface of bastnaesite minerals before and after the action of reagents: (a) O1s, (b) N1s

mixed metal ions $\text{Ca}^{2+}/\text{Fe}^{3+}$, $\text{Ca}^{2+}/\text{Ba}^{2+}$, and $\text{Ca}^{2+}/\text{Ba}^{2+}/\text{Fe}^{3+}$ were used to treat the bastnaesite. The O1 s spectrum of the adsorption of OHA showed that the photoelectron intensity of the O1 s spectrum was lower than that of the surface O1 s spectrum of the bastnaesite without metal ion treatment, indicating that the metal ions and OHA were adsorbed on the surface of the bastnaesite at the same time, reducing the relative concentration of the O element on the surface of the original bastnaesite, which indicated that the metal ions promoted the adsorption of OHA on the bastnaesite and increased the adsorption amount of OHA.

Fig. 6(b) shows the fitting spectrum of N1 s narrow spectrum on the surface of bastnaesite after the action of reagents. It can be seen from the O1 s spectrum of bastnaesite only treated with OHA that two fitting peaks are obtained by fitting, which are located at 400.71 eV and 398.85 eV. The 400.71 eV is the N-C chemical bond, while the 398.85 eV is the N-O chemical bond. Combined with the fitting analysis of Ce3 d, C1 s, and O1 s, the mechanism of the interaction between bastnaesite and OHA collector is revealed. The molecular hydroxamic acid R-CO-NH-OH has physical adsorption with bastnaesite. The ionic state of R-CO-NH-OH chemically adsorbs with bastnaesite, and the N atom of hydroxamic acid provides electrons to chelate with the Ce atom on the surface of bastnaesite to form a stable five-membered ring chelate. When single metal ions Ca^{2+} , Ba^{2+} , Fe^{3+} and mixed metal ions $\text{Ca}^{2+}/\text{Fe}^{3+}$, $\text{Ca}^{2+}/\text{Ba}^{2+}$, and $\text{Ca}^{2+}/\text{Ba}^{2+}/\text{Fe}^{3+}$ acted on bastnaesite, the N1s peak pattern adsorbed on the surface of bastnaesite changed, indicating that the addition of metal ions affected the form of OHA collector adsorbed by bastnaesite. The introduction of single metal ions will strengthen the adsorption of OHA by bastnaesite. Among them, the introduction of Ba^{2+} promotes the adsorption of OHA by bastnaesite to the maximum, followed by Fe^{3+} and Ca^{2+} .

It can be seen from Fig. 7 that there are orbital peaks of metal elements on the surface of bastnaesite, which can fully explain that the surface of bastnaesite adsorbs metal ions Ca^{2+} , Ba^{2+} , and Fe^{3+} . Fig. 7(1)-7(3) are the orbital peaks of metal elements on the surface of bastnaesite when single metal ions Ca^{2+} , Ba^{2+} , and Fe^{3+} act on the surface of bastnaesite respectively. It can be seen from Fig. 7(a) that the characteristic peak of $\text{Ca}2p_{3/2}$ is at 346.86 eV, and the characteristic peak of $\text{Ca}2p_{1/2}$ is at 350.45 eV. Fig. 7(b) shows that the characteristic peak of $\text{Ba}3d_{5/2}$ is at 779.50 eV, the characteristic peak of $\text{Ba}3d_{3/2}$ is at

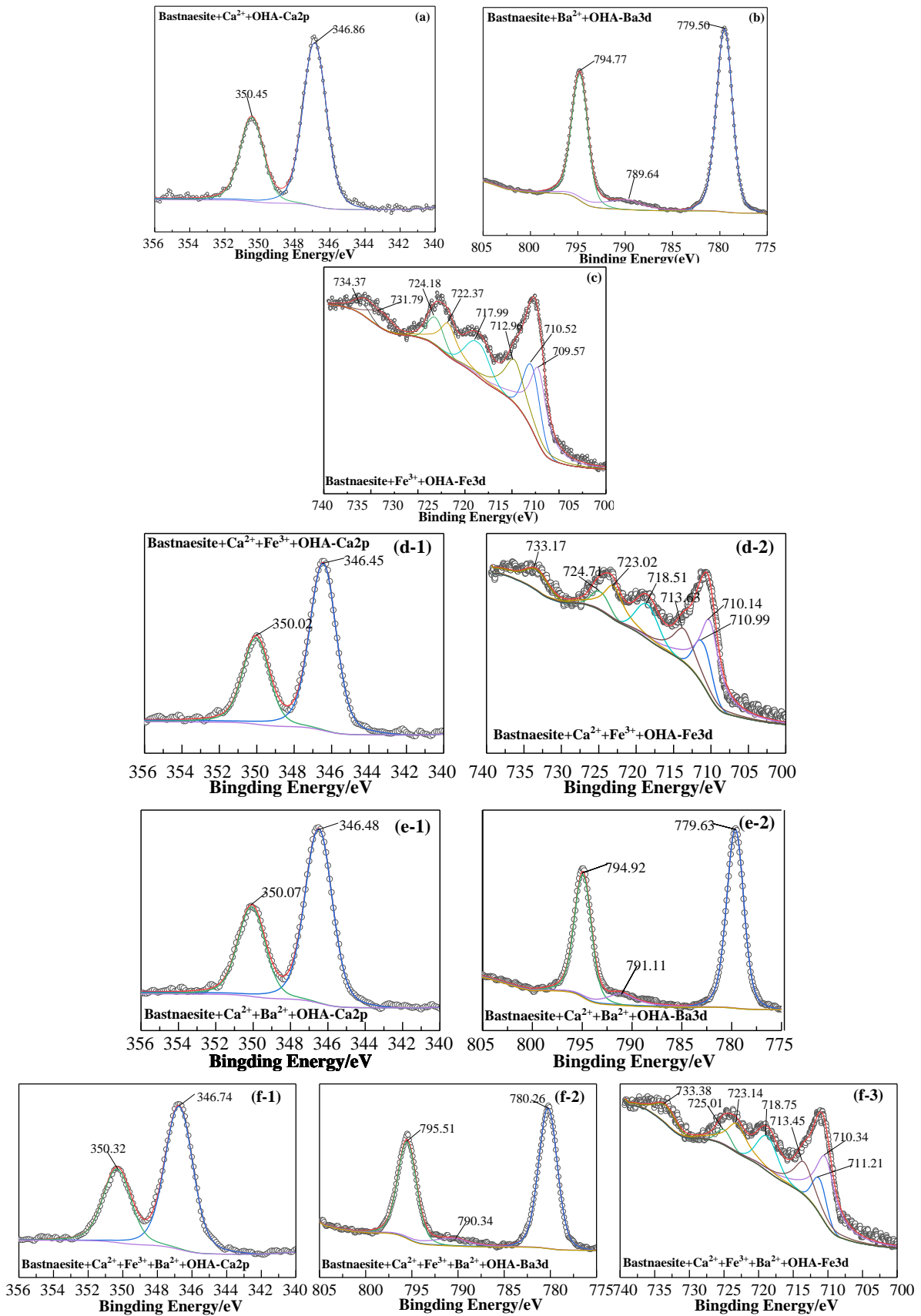


Fig. 7. The narrow-spectrum scanning fitting spectrum of metal elements on the surface of bastnaesite before and after the action of reagents: (a) Ca2p; (b) Ba3d; (c) Fe3d; (d-1) Ca2p; (d-2) Fe3d; (e-1) Ca2p; (e-2) Ba3d; (f-1) Ca2p; (f-2) Ba2p; (f-3) Fe3d

794.77 eV, and the chemical bond of Ba-N may be at 789.64 eV, which is the reaction of OHA with Ba^{2+} , the dominant component of Ba^{2+} , to form a metal chelate.

It can be seen from Fig. 7(c) that 710.52 eV and 712.90 eV are the characteristic peaks of $\text{Fe}3d_{3/2}$, 724.18 eV and 723.37 eV are the characteristic peaks of $\text{Fe}3d_{1/2}$, and 717.99 eV may be the chemical bond of Fe-N, which is the reaction of OHA with $\text{Fe}(\text{OH})^{2+}$, the dominant component of Fe^{3+} , to form metal chelates. Fig. 7(d-1) and Fig. 7(d-2) are the Ca2p orbital peak and Fe2p orbital peak appearing on the surface of bastnaesite due to the interaction of mixed metal ions $\text{Ca}^{2+}/\text{Fe}^{3+}$, which indicates that the two metal ions interact with the surface of bastnaesite at the same time. Similarly, Fig. 7(e-1) and Fig. 7(e-2) are the Ca2p orbital peak and the Ba3d orbital peak appearing on the surface of the bastnaesite due to the $\text{Ca}^{2+}/\text{Ba}^{2+}$ interaction of the mixed metal ions, which indicates that the two metal ions interact with the surface of the bastnaesite at the same time. The mixed metal ions $\text{Ca}^{2+}/\text{Ba}^{2+}/\text{Fe}^{3+}$ interact with the surface of bastnaesite, and Ca2p orbital peak, Ba3d orbital peak, and Fe2p orbital peak appear, as shown in Fig. 7(f-1), 7(f-2), and 7(f-3), which indicates that the three metal ions interact with the surface of bastnaesite at the same time. Combined with the flotation test and adsorption capacity test, it can be seen that the mixed metal ions are adsorbed on the surface of bastnaesite, which hinders the adsorption of OHA.

3.1.4. DFT study on the adsorption of OHA on bastnaesite surface by metal ions

The DFT calculation of the surface adsorption of bastnaesite before and after metal ion doping was performed using the quantum chemical calculation program CASTEP. The external valence electron arrangements of the nuclei involved in the calculation were O $2s_22p_4$, C $2s_22p_2$, F $2s_22p_5$, Ce $4f_15s_25p_65d_16s_2$, Fe $3s_24p_63s_5$, Ca $3s_24p_64s_2$, Ba $5s_25p_66s_2$. Researchers (Espiritu ERL et al., 2018; Moonchul et al., 2022; Tian et al., 2022; Yu et al., 2023) have shown that the (100) crystal plane of bastnaesite is dissociated after crushing and grinding of bastnaesite, and the (100) crystal plane is the main adsorption surface of flotation reagents. Therefore, the (100) surface of bastnaesite is selected as the research object, as shown in Fig. 8, which is the most stable model of OHA adsorption on the (100) surface of bastnaesite before and after metal ion doping.

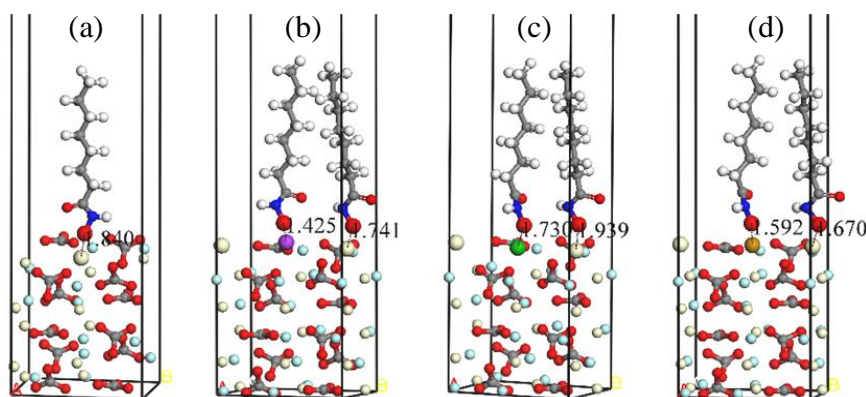


Fig. 8. The most stable adsorption model on the (100) surface of bastnaesite before and after metal ion doping: (a) bastnaesite + OHA; (b) bastnaesite + Fe^{3+} + OHA; (c) bastnaesite + Ca^{2+} + OHA; (d) Bastnaesite + Ba^{2+} + OHA

It can be seen from Fig. 8(a) that when there is no metal atom doping, the Ce atom on the surface of the bastnaesite interacts with the oxygen atom on the OHA anion to form a bond, and the bond length of Ce-O is 1.840 Å. After Fe is adsorbed on the surface of bastnaesite, as shown in Fig. 8(b), two kinds of interaction bonds are formed on the surface of bastnaesite. One is the interaction between Ce atom and oxygen atom on OHA anion, and the bond length of Ce-O is 1.741 Å. The other is the interaction between Fe atom and oxygen atom on OHA anion, and the bond length of Fe-O is 1.425 Å. After Ca is adsorbed on the surface of bastnaesite, as shown in Fig. 8(c), two kinds of interaction bonds are formed on the surface of bastnaesite. One is the interaction between Ce atom and oxygen atom on OHA anion, and the bond length of Ce-O is 1.939 Å. The other is the interaction between Ca atom and oxygen atom on OHA anion, and the bond length of Ca-O is 1.730 Å. After Ba is adsorbed on the surface of bastnaesite, as shown in Fig. 8(d), two kinds of interaction bonds are formed on the surface of bastnaesite. One is

the interaction between Ce atom and oxygen atom on OHA anion, and the bond length of Ce-O is 1.670 Å. The other is the interaction between Ba atom and oxygen atom on OHA anion, and the bond length of Ba-O is 1.502 Å. By comparison, it can be found that after Fe atoms are adsorbed on the surface of bastnaesite, the distance between Ce, Fe atoms on the surface of bastnaesite and oxygen atoms on OHA anions is significantly smaller than that between metal ions adsorbed on the surface of bastnaesite by Ca and Ba atoms and oxygen atoms on OHA. This also proves that the adsorbed metal ions of bastnaesite affect the bonding between OHA and metal ions on the surface of bastnaesite, which in turn affects the interaction between reagents and minerals.

In order to further study the adsorption mechanism of metal ions on the surface of bastnaesite to adsorb OHA, the first-principles method based on density functional theory was used to simulate the process of metal ions replacing the lattice surface of bastnaesite Ce atoms and adsorbing with OHA. The adsorption process on the surface of bastnaesite was studied at the atomic level, which provided a theoretical reference for the flotation of bastnaesite.

In order to understand the adsorption energy reaction on the surface of bastnaesite before and after impurity metal ion doping, it can be calculated by Eq. (1) (Tian et al., 2018):

$$E_{\text{ads}} = E_{\text{Slab+MI}} - E_{\text{Slab}} - E_{\text{MI}} \quad (1)$$

In Eq. (1), E_{ads} is the adsorption energy of metal ions on the mineral surface, $E_{\text{Slab+MI}}$ is the total energy of the adsorption model of metal ions on the mineral surface after structural optimization, E_{Slab} represents the energy of the Slab model on the mineral surface, and E_{MI} is the energy of OHA ions.

The calculation formula of the adsorption energy of the reagent on the mineral surface (1), and the calculation results of the adsorption energy of the interaction between OHA and bastnaesite (100) surface before and after metal ion doping are shown in Table 3.

It can be seen from Table 3 that when there is no metal ion doping, the adsorption energy of bastnaesite and OHA is -386.8636 kJ/mol, indicating that OHA can spontaneously adsorb on the surface of bastnaesite, resulting in the hydrophobicity of the surface of bastnaesite, which is beneficial to the flotation of bastnaesite. The adsorption energy between the surface of bastnaesite doped with Fe and OHA is -485.3819 kJ/mol, the adsorption energy between the surface of bastnaesite doped with Ca and OHA is -453.7552 kJ/mol, and the adsorption energy between the surface of bastnaesite doped with Ba and OHA is -492.6347 kJ/mol. It shows that with the addition of metal ions, because the adsorption energy of OHA and bastnaesite surface is reduced, its spontaneity is stronger and its adsorption capacity is enhanced. It can be further reflected that the effect of metal ions on the surface ability of OHA to adsorb bastnaesite is Ba^{2+} , Fe^{3+} , and Ca^{2+} . This result is consistent with the flotation behavior and detection analysis results.

Table 3. Adsorption energy of interaction between OHA and bastnaesite (100) surface before and after metal ion doping

Interaction state	Adsorption Energy (kJ/mol)
Bastnaesite + OHA	-386.8636
Bastnaesite + Fe^{3+} + OHA	-485.3819
Bastnaesite + Ca^{2+} + OHA	-453.7552
Bastnaesite + Ba^{2+} + OHA	-492.6347

The adsorption mechanism of OHA on bastnaesite (100) surface was discussed by analyzing the total density of states of OHA on bastnaesite (100) surface before and after metal ion doping, as well as the partial density of states of Ce, O, Fe, Ca and Ba atoms and Mulliken charge population changes. The total density of states of the interaction between OHA and bastnaesite (100) surface before and after metal ion doping and the partial density of states of each atom are shown in Fig. 9. The Mulliken charge distribution before and after the adsorption of O, Ce, Fe, Ca, and Ba atoms is shown in Table 4. The chemical bond length and Mulliken layout of the (100) surface of bastnaesite before and after the action of metal ions are shown in Table 5.

It can be seen from Fig. 9 that the total state density of the surface change of bastnaesite and the change of the partial density of states of each atom. From the total state density of bastnaesite in (a), it

can be found that the addition of metal ions leads to the change of the peak shape of the total state density, indicating that the addition of metal ions changes the adsorption mode of bastnaesite and OHA.

In Fig. 9(b), the partial density of states of Ce atoms interacting with OHA on the surface of bastnaesite before and after metal ion doping can be found. Before metal ion doping, 5s, 5d, and 5d orbitals provide the main contribution to the density of states peak near the Fermi level, and cross the Fermi level, indicating that the reactivity of Ce atoms before adsorption is provided by 5s, 5d, and 5d orbitals. After the doping of impurity metal ions, the density of the state peak of Ce atom above the Fermi level also shows a trend of moving in the direction of low energy, indicating that the doping of metal ions leads to the occurrence of this phenomenon. In Fig. 9(c), the partial density of states of O atoms interacting with OHA before metal ion doping on bastnaesite surface. The 2p orbital provides the main contribution to the density of states peak near the Fermi level, and the density of states peaks of some 2p orbitals cross the Fermi level and enter the conduction band region, indicating that the activity of O atoms before adsorption is strong, and its activity is mainly provided by the 2p orbital. After the adsorption of impurity metal ions on the surface of bastnaesite, the state density peak of O atom moves to the direction of higher energy, and the non-locality of state density in the energy range of $-30\sim 0$ eV increases obviously. The strong 'resonance' in the energy range of $-30\sim 0$ eV was observed in the density

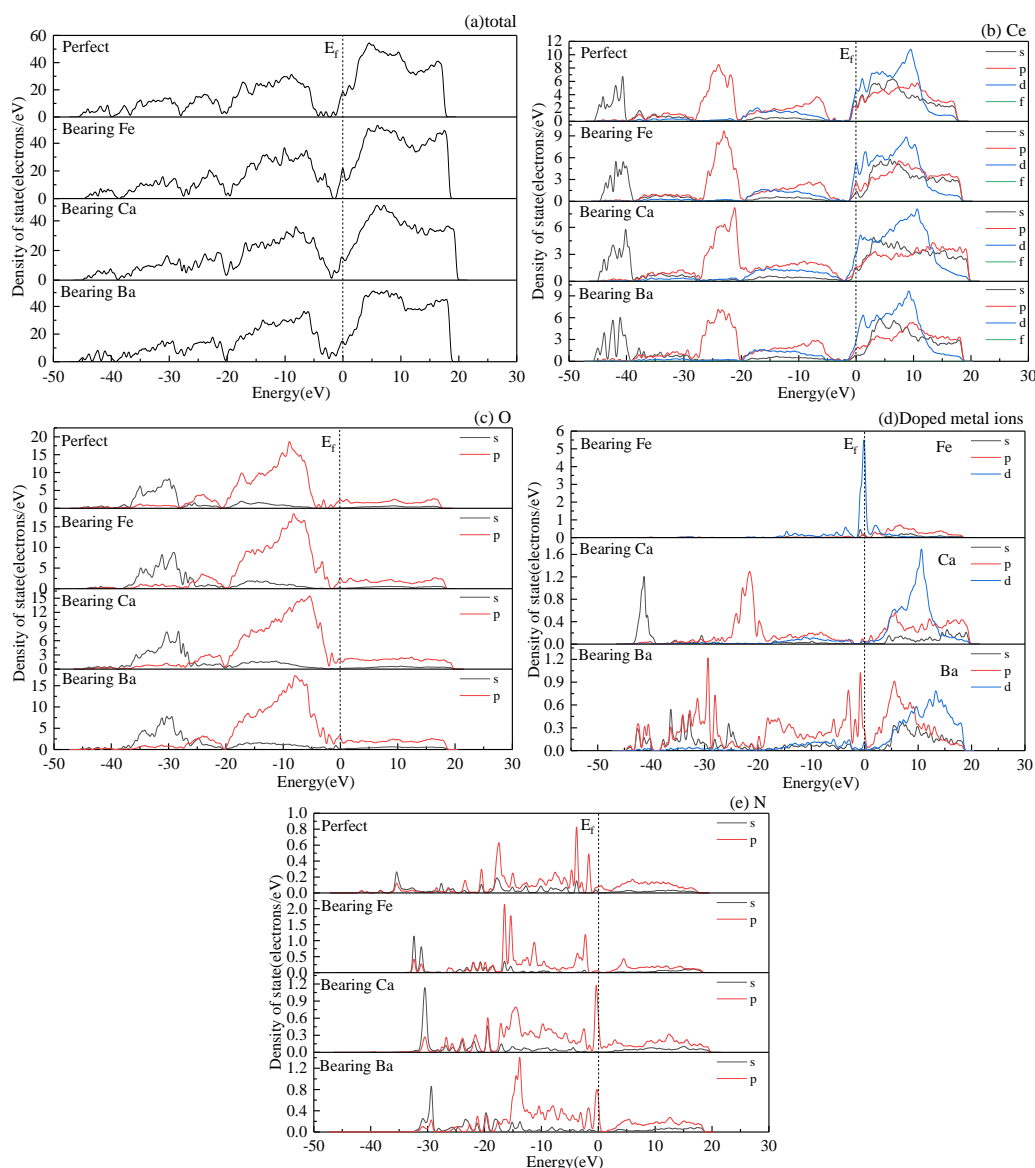


Fig. 9. The total density of states and the partial density of states of each atom in the interaction between OHA and bastnaesite (100) surface before and after metal ion doping: (a) total density of states; (b) Ce; (c) O; (d) Doped metal atoms; (e) N

of states (DOS) peak of O atom and Ce atom and impurity metal atom after adsorption, indicating that chemical bonds were formed between O atom and Ce atom and impurity Fe, Ca, and Ba atoms. It can be seen from Fig. 9(d) that the density of states of the impurity metal atoms appears. The density of states peak of the Fe atom shows that the 3d orbital provides a major contribution to the density of states peak near the Fermi level, in which the 3d orbital crosses the Fermi level, indicating that the reaction activity of the Fe atom after adsorption is provided by the 3d orbital. The density of states peak of Ca atom shows that the density of states peak near the Fermi level is not obvious, and the orbit entering the conduction band is composed of 4p and 4d orbits, indicating that the reactivity of Ca atom after adsorption is provided by 4p and 4d orbits. The density of states peak of Ba atom shows that the 5p orbital provides the main contribution to the density of states peak near the Fermi level, and the 5p and 6d orbitals cross the Fermi level, indicating that the reactivity of Ba atom after adsorption is provided by the 5p and 6d orbitals.

Fig. 9 shows the partial density of states of N atoms interacting with OHA before and after the doping of impurity metal ions on the surface of bastnaesite. It can be seen from the density of states peak that the peak shape has changed. Before the doping of impurity metal ions, the peak of the partial density of states of N atoms interacting with OHA is sharp and the range is small. After the doping of impurity metal ions, the energy of the density of states of N atoms moves higher, the s orbital peak near -30 eV becomes higher, and the density of states peak at -20~0 eV overlaps, indicating that the appearance of covalent bonds may be caused by impurity metal atoms Fe, Ca, and Ba. It can be seen from the above data analysis that when the doped impurity metal atoms are added, there are two adsorption forms on the surface of bastnaesite and OHA, one is R-NH-O-M-CeFCO₃ and R-NH-O-CeFCO₃.

Table 4. Mulliken charge distribution of OHA interacting with bastnaesite (100) surface before and after metal ion doping

Interaction State	Atomic Species	s	p	d	f	Total	Charge (e)
Bastnaesite + OHA	Ce2	2.32	5.25	2.21	0.00	9.79	2.21
	O39	1.73	4.82	0.00	0.00	6.55	-0.55
	N1	1.48	3.90	0.00	0.00	5.38	-0.38
Bastnaesite + Fe ³⁺ + OHA	Ce2	1.49	5.52	2.19	0.00	9.20	2.80
	O39	1.74	4.81	0.00	0.00	6.55	-0.55
	Fe	0.51	0.34	7.07	0.00	7.92	0.08
	O37	1.72	4.59	0.00	0.00	6.32	-0.32
	N1	1.32	4.02	0.00	0.00	5.34	-0.34
	N2	1.34	4.03	0.00	0.00	5.37	-0.37
Bastnaesite + Ca ²⁺ + OHA	Ce2	1.31	5.55	1.98	0.00	8.85	3.15
	O39	1.83	4.70	0.00	0.00	6.63	-0.53
	Ca	2.13	5.43	1.27	0.00	8.83	1.17
	O37	1.76	4.75	0.00	0.00	6.51	-0.51
	N1	1.34	3.93	0.00	0.00	5.26	-0.26
	N2	1.37	3.94	0.00	0.00	5.31	-0.31
Bastnaesite + Ba ²⁺ + OHA	Ce2	1.35	4.67	2.10	0.00	7.97	4.03
	O39	1.75	4.77	0.00	0.00	6.52	-0.52
	Ba	2.13	5.62	1.62	0.00	9.37	0.63
	O37	1.83	4.72	0.00	0.00	6.55	-0.55
	N1	1.35	4.02	0.00	0.00	5.37	-0.37
	N2	1.39	4.01	0.00	0.00	5.40	-0.40

The Mulliken charge distribution of OHA interacting with the (100) surface of bastnaesite before and after impurity metal ion doping is shown in Table 4. After the interaction between OHA and bastnaesite surface before doping, the total charge of Ce2 is 9.79 e, the total charge of O39 is 6.55 e, the total charge of N1 is 5.38 e, and the total charge of N1 is 0.38 e. Ce2 is the electron donor, while O39 and N1 are the electron acceptors, which can reflect that Ce8 on the surface of bastnaesite forms a chemical bond with O67 on OHA. From Table 5, it can be seen that the layout value of C2-O39 chemical bond is 0.24, and

the bond length is 1.49292 Å.

When the Fe atom doped bastnaesite surface interacts with OHA, the total charge of Ce2 is reduced to 9.20 e and 2.80 e is lost, while Fe loses 0.08 electrons. The total charge of O39 is 6.55 e, the total charge of O37 is 6.32 e, the total charge of N1 is 5.34 e, the total charge of N2 is 5.37 e, and the total charge of N2 is -0.37 e. It can be seen that Ce8 and Fe are electron donors, while O67, O65, N1, and N2 are electron acceptors, indicating that Ce8 and Fe on the surface of bastnaesite form chemical bonds with O67 and O65 on OHA.

Table 5. Chemical bond length and Mulliken population of OHA with bastnaesite (100) surface before and after metal ion doping.

Interaction State	Chemical Bond	Layout Value	Bond Length (Å)
Bastnaesite + OHA	Ce2–O39	0.24	1.49292
Bastnaesite + Fe ³⁺ + OHA	Ce2–O39	0.14	1.74051
	Fe–O37	0.68	1.42518
Bastnaesite + Ca ²⁺ + OHA	Ce2–O39	0.01	1.93883
	Ca–O37	0.13	1.72975
Bastnaesite + Ba ²⁺ + OHA	Ce2–O39	0.12	1.67006
	Ba–O37	0.21	1.59229

As can be seen from Table 5 that the layout value of Ce2-O39 increases to 0.14, the bond length increases to 1.74051 Å, and a new chemical bond Fe-O37 is generated. The layout value is 0.68 and the bond length is 1.42518 Å. It can be seen that the ionic bond of Ce2-O39 is enhanced and the bond is easy to break, while the covalent bond of Fe-O37 is enhanced and the bond is not easy to break. It can be explained that Fe atom doping is beneficial to the adsorption of OHA on the surface of bastnaesite. Similarly, after Ca and Ba atoms doped with bastnaesite surface interact with OHA, the electrons of Ce2 lose more, while Ca and Ba atoms lose electrons, while O39, O37, N1, and N2 get more electrons. The specific data can be seen in Tables 4 and 5. In addition to the formation of Ce2-O39 chemical bonds on the surface of bastnaesite, there is also the formation of Ca-O37 and Ba-O37 chemical bonds. Therefore, the impurity metal adsorbs on the surface of the bastnaesite to form a chemical bond and adsorbs OHA together with the Ce atom present on the surface of the bastnaesite. The diversified chemical adsorption method is denser and not easy to fall off. The content of N element on the surface of the bastnaesite increases, which is beneficial to the flotation of the bastnaesite. It further reflects that the impurity metal atoms are doped on the surface of bastnaesite, which is beneficial to the flotation of bastnaesite. This result is confirmed by flotation, adsorption capacity test, and XPS analysis of bastnaesite.

3.2. Discussion

The (100) crystal plane of bastnaesite is more cleavage, and a large number of dominant cleavage planes are exposed during the grinding process, which are the main adsorption surfaces of flotation reagents. It can be seen from the first principles that the carbonates in the (100) crystal plane of the bastnaesite are alternately arranged with fluorine atoms and cerium atoms, and the Ce atoms are chemically active.

In this study, when there is no metal ion in the bastnaesite pulp, the OHA collector is mainly adsorbed on the surface of the bastnaesite by two oxygen atoms and cerium atoms to form a five-membered chelate, as shown in Fig. 10. The oxygen atoms on the surface did not act as adsorption sites, resulting in the collector not being uniformly adsorbed on the surface of the bastnaesite. XPS shows that the relative content of N atoms adsorbed on the surface of bastnaesite is small.

Through the analysis of the detection before and after the action of bastnaesite and the DFT study of the (100) surface, it is concluded that there are two adsorption sites of bastnaesite. One is that the Ce atom adsorbs the two oxygen atoms of OHA to form a five-membered chelate, and the other is that the O-M(OH) on the bastnaesite interacts with OHA; By comparing the different pulp environments, the binding energy of the N1 s peak adsorbed by the bastnaesite is quite different, indicating that the N atom plays a chemical bonding role. Therefore, it is inferred that the configuration of the oxygen atom adsorption site is O-M-O-N bonding. During the period, M(OH)^{n+(n:1,2)} loses OH⁻, while the N-O-H

chemical bond on OHA loses H^+ , forming an H_2O molecule. The typical dehydration reaction is more stable, and the adsorption configuration is shown in Fig. 11. From the above conclusions, it can be concluded that the impurity metal ions can be adsorbed on the surface of bastnaesite by ion exchange or directly combined with the lattice ions on the mineral surface, interact with OHA, and form M-OHA chelate by chemical adsorption to promote the further adsorption of collector OHA, which exceeds the adsorption effect when OHA is used alone and effectively improves the floatability of bastnaesite.

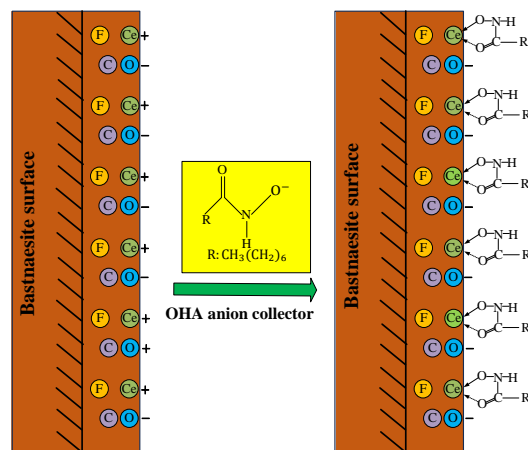


Fig. 10. Schematic diagram of adsorption configuration of OHA adsorbed by bastnaesite flotation

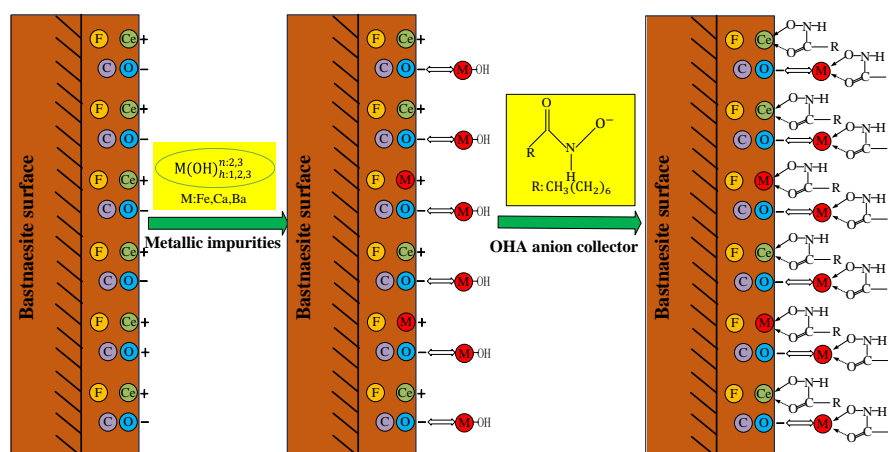


Fig. 11. Schematic diagram of adsorption configuration of OHA on bastnaesite flotation treated by metal ions (M: Fe³⁺, Ca²⁺, Ba²⁺)

5. Conclusions

In this study, the influence mechanism of metal ions on the adsorption of OHA by bastnaesite was studied by flotation test, adsorption capacity test, XPS analysis, and DFT study. The conclusions are as follows:

The flotation test shows that the ability to promote the recovery rate of bastnaesite is $Ba^{2+} > Fe^{3+} > Ca^{2+}$. The addition of mixed metal ions will inhibit the flotation recovery rate of bastnaesite. It may be that the increase of metal ion concentration will lead to competitive adsorption, and inhibit the adsorption of OHA on the surface of bastnaesite, and the decrease of hydrophobicity of bastnaesite surface will lead to the decrease of recovery rate.

The adsorption experiments show that single metal ions can promote the adsorption of OHA on bastnaesite, especially Ba^{2+} has the largest adsorption capacity on bastnaesite, while mixed metal ions are unfavorable to the adsorption of OHA on the surface of bastnaesite, inhibiting the adsorption of OHA on the surface of bastnaesite.

XPS showed that Ca, Ba, and Fe elements appeared after the action of single metal ions, and two or three metal ion elements appeared at the same time after the action of mixed metal ions. The N

concentration on the surface of bastnaesite after the action of single metal ions is significantly higher than that without metal ions, while the N concentration on the surface of bastnaesite after the action of mixed metal ions is significantly lower than that without metal ions. When metal ions and OHA are introduced into bastnaesite, the surface O1s of bastnaesite consists of three peaks, which are from O-M (M is a metal atom), O-N, and Ce-O, respectively. O-M bond is the dominant component of metal ions adsorbed on the surface of bastnaesite, forming Ca-O, Ba-O, and Fe-O chemical bonds. When Ca^{2+} is added, a new peak appears at 401.24 eV in the N1s fitting peak, which may be caused by the formation of N-Ca(OH) chemical bond between $\text{Ca}(\text{OH})^+$ and nitrogen atoms in OHA. When Ba^{2+} and Fe^{3+} are added, new peaks appear at 397.68 eV and 397.19 eV in the fitting peak of N1s, which may be caused by nitrogen, which is N-Ba(OH) and N-Fe(OH), respectively, indicating that metal ions Ba^{2+} and Fe^{3+} form metal chelates with nitrogen atoms in OHA.

The DFT study of the (100) surface of bastnaesite shows that when there is no metal ion doping, the adsorption energy of bastnaesite and OHA is -386.8636 kJ/mol, the adsorption energy of Fe-doped bastnaesite surface and OHA is -485.3819 kJ/mol, the adsorption energy of Ca-doped bastnaesite and OHA is -453.7552 kJ/mol, and the adsorption energy of Ba-doped bastnaesite and OHA is -492.6347 kJ/mol. It shows that with the addition of metal ions, because the adsorption energy of OHA and bastnaesite surface is reduced, its spontaneity is stronger and its adsorption capacity is enhanced. There are two adsorption sites on bastnaesite. One is that Ce atom adsorbs two oxygen atoms of OHA to form a five-membered chelate, and the other is that the O-M(OH) on bastnaesite interacts with OHA. Therefore, it is inferred that the configuration of the oxygen atom adsorption site is O-M-O-N bond, during which $\text{M}(\text{OH})^{n+}$ ($n=1,2$) loses OH^- , and the N-O-H chemical bond on OHA loses H^+ to form a H_2O molecule, a typical dehydration reaction, so the adsorption is more stable. Through comprehensive flotation test, adsorption capacity test, XPS analysis, and DFT analysis, it is concluded that the addition of doped impurity metal atoms leads to two adsorption forms between the surface of bastnaesite and OHA, one is R-NH-O-M-Ce FCO_3 and R-NH-O-Ce FCO_3 .

Acknowledgments

The study was funded by the Inner Mongolia Autonomous Region Science and Technology Plan Project (Grant No.2021GG0438), Inner Mongolia Natural Science Foundation (2020MS05048, 2020BS05029), and Fund Project National Key R & D Program (Rare Earth Based Solid Waste Resource Properties, Precision Mining and Ecological Environmental Impact Assessment) (2020YFC1909101).

References

- BUDI, A., STIPP, S.L.S., ANDERSSON, M.P., 2018. *Calculation of entropy of adsorption for small molecules on mineral surfaces*. J. Phys. Chem. 122, 8236–8243.
- CAO, S.M., CAO, Y.J., MA, Z.L., LIAO, Y.F., 2018. *Metal ion release in bastnaesite flotation system and implications for flotation*. Minerals. 8(5), 203.
- CAO, S.M., CAO, Y.J., MA, Z.L., LIAO, Y.F., 2019. *The adsorption mechanism of Al(III) and Fe(III) ions on bastnaesite surfaces*. Physicochem. Probl. Miner. Process. 55 (1), 97–107.
- CAO, Z., CAO, Y.D., QU, Q.Q., ZHANG, J.S., MU, Y.F., 2019. *Separation of bastnaesite from fluorite using ethylenediamine tetraacetic acid as depressant*. Miner. Eng. 134, 134–141.
- CHEN, L.Z., HOU, Q.L., YIN, R.M., 2012. *The mechanism of calcium ions effects on quartz collection in the system of dodecyl sulphonate*. Journal of Hunan University of Technology. 26(6), 8–12.
- CHEN, P., ZHAI, J.H., SUN, W., HU, Y.H., YIN, Z.G., 2017. *The activation mechanism of lead ions in the flotation of ilmenite using sodium oleate as a collector*. Miner. Eng. 111, 100–107.
- DÁVILA-PULIDO, I.G., URIBE-SALAS, A., ÁLVAREZ-SILVA METAL., 2015. *The role of calcium in xanthate adsorption onto sphalerite*. Miner. Eng. 71, 113–119.
- DUSHYANTHA, N., BATAPOLA, N., ILANKOON, I.M.S.K., ROHITHA, S., PREMASIRI, R., ABEYSINGHE, B., RATNAYAKE, N., DISSANAYAKE, K., 2020. *The story of rare earth elements (REEs): Occurrences, global distribution, genesis, geology, mineralogy and global production*. Ore Geol. Rev. 122, 103521.
- ESPIRITU ERL, DA SILVA GR, AZIZI D, LARACHI F, WATERS KE., 2018. *The effect of dissolved mineral species on bastnaesite, monazite and dolomite flotation using benzohydroxamate collector*. Colloids and Surfaces A: Physicochemical and Engineering Aspects. 539, 31934.

- GAO, Y.S., GAO, Z.Y., SUN, W., 2017. *Research progress of influence of metal ions on mineral flotation behavior and underlying mechanism*. The Chinese Journal of Nonferrous Metals. 27(4), 859–868.
- GAO, Z., JIANG Z., SUN, W., YUE, S., 2021. *Typical roles of metal ions in mineral flotation: A review*. Transactions of Nonferrous Metals Society of China., 31(7), 2081-2101.
- HUANG, W.X., LIU, W.B., ZHONG, W.L., 2021. *Effects of common ions on the flotation of fluorapatite and dolomite with oleate collector*. Miner. Eng. 174, 107213.
- JORDENS, A., CHENG, Y., WATERS, K.E., 2013. *A review of the beneficiation of rare earth element bearing minerals*. Miner. Eng. 41, 97-114.
- LI, N., MA, Y, WANG, Q.W., HOU, S.H., LI, E.D., WANG, J.J., 2019. *Spectroscopic Study on the Interaction between Baiyunobo Rare Earth Minerals and Hydroxamic Acid Collector*. Chinese Rare Earths. 553, 210-219.
- LIN, Y.M., CHEN, C., WANG, W.Q., JIANG, Y., CAO, X., 2020. *Beneficial effects and mechanism of lead ions for bastnaesite flotation with octyl hydroxamic acid collector*. Miner. Eng. 148, 106199.
- LIU, M., CHEN, J.H., CHEN, Y., ZHU, Y.G., 2020. *Interaction between smithsonite and carboxyl collectors with different molecular structure in the presence of water: A theoretical and experimental study*. Appl. Surf. Sci. 510, 145410.
- LIU, C., 2023. *A review of flotation reagents for bastnäsite-(Ce) rare earth ore*. Advances in Colloid and Interface Science. 321, 103029.
- LONG, K.R., GOSEN, B.S.V., FOLEY, N.K., CORDIER, D., 2012. *The principal rare earth elements deposits of the United States: A Summary of domestic deposits and a global perspective*, Springer. Dordrecht, The Netherlands. 131-155.
- MOONCHUL, J., BOGALE, T., CRAIG, D., 2022. *Influence of monovalent and divalent cations on monazite flotation*. Colloids and Surfaces A: Physicochemical and Engineering Aspects. 653.
- QI, J., FAN, H.L., LIU, G.Y., 2020. *β -Amino-hydroxamate surfactants: Preparation, and adsorption mechanism in bastnaesite flotation*. Sep. Purif. Technol. 240, 116634.
- SRINIVASAN, S.G., SHIVARAMAIAH, R., KENT, P.R.C., STACK, A.G., NAVROTSKY, A., RIMMAN, R.E., ANDERKO, A., BRYANTSEV, VS., 2016. *crystal structures, surface stability, and water adsorption energies of la-bastnäsite via density functional theory and experimental studies*. J. Phys. Chem. 120(30), 16767-16781.
- TIAN, M.G., LIU, R.Q., GAO, Z.Y., CHEN, P., HAN, H.S., WANG, L., ZHANG, C.Y., SUN, W., HU, Y.H., 2018. *Activation mechanism of Fe (III) ions in cassiterite flotation with benzohydroxamic acid collector*. Miner. Eng. 119, 31-37.
- WANG, Z.J., WU, H.Q., XU, Y.B., SHU, K.Q., FANG, S., XU, L.H., 2020. *The effect of dissolved calcite species on the flotation of bastnaesite using sodium oleate*. Miner. Eng. 145, 106095.
- WANHALA., ANNA K., DOUGHTY, BENJAMIN, BRYANTSEV, VYACHESLAV S., WU., LILI, MAHURIN., SHANNON M., JANSONE- POPOVA., SANTA., CHESHIRE., MICHAEL C., NAVROTSKY., ALEXANDRA., STACK., ANDREW G., 2019. *Adsorption mechanism of alkyl hydroxamic acid onto bastnäsite: Fundamental steps toward rational collector design for rare earth elements*. J. Colloid Interface Sci. 553, 210-219.
- WEI, Q., DONG, L.Y., JIAO, F., QIN, W.Q., 2019. *Use of citric acid and Fe(III) mixture as depressant in calcite flotation*. Colloids Surf. 578, 123579.
- XU, Y., XU, L., WU, H., WANG, Z., SHU, K., FANG, S., ZHANG, Z., 2020. *Flotation and co-adsorption of mixed collectors octano hydroxamic acid/sodium oleate on bastnaesite*. Journal of Alloys and Compounds. 819, 152948.
- XU, L., LIU, B., JIAO, H., GAO, S.L., 2023. *Research progress of coordination effect in flotation capture reagents of rare earth ore*. Chinese Journal of Chemical Education. 44(22):7-13.
- YIN, W.Z., TANG, Y., 2021. *Current Status in Study of Genetic Flotation of Minerals*. Metal Mine. 01, 42-54.
- YU, X.Y., ZHANG, R.R., YANG, S.Y., LIU, C., HE, G.C., WANG, H.L., WANG, J.L., 2020. *A novel decanedioic hydroxamic acid collector for the flotation separation of bastnäsite from calcite*. Miner. Eng. 151, 106306.
- YU, L., XIN, Y., YUAN, Z.T., 2022. *Effect of lead ions on the selective flotation of ilmenite against titanite using octyl hydroxamic acid as collector*. Applied Surface Science. 603,154458.
- YU, A.M., DING, Z., LI, J., YUAN, J.Q., BAI, S.J., 2023. *Research progress on activation mechanism of typical metal ions on mineral flotation*. Conservation and Utilization of Mineral Resources. 43(04),114-122.
- ZHANG, J.X., FENG, Y.L., NIU, F.S., 2014. *Influence of metal ions in pulp on floatability of kyanite minerals*. Journal of Northeastern University. Natural Science. 35(12),1787-1791.
- ZHENG, Q., QIAN, Y., ZOU, D., 2021. *Surface mechanism of Fe³⁺ ions on the improvement of fine monazite flotation with octyl hydroxamate as the collector*. Frontiers in Chemistry. 9, 700347.